LIQUEFACTION SUSCEPTIBILITY BASED ON DISSIPATED ENERGY: A CONSISTENT DESIGN METHODOLOGY

R. O. Davis [1], J. B. Berrill [1,2]

ABSTRACT

This paper presents a novel approach to characterization of liquefaction susceptibility for deposits of saturated cohesionless soils. The method we propose is based on an assumed relationship between pore pressure increase and dissipated energy density within the soil layer. Use of dissipated energy is not new. What makes the present work different is our approach to the energy calculation. Earlier analyses used simple attenuation models based on earthquake magnitude and epicentral distance to determine the dissipated energy and hence the pore pressure increase within a sand deposit. In this work, instead of magnitude and distance, we will use the response spectrum for surface motion at the site as input information. This permits us to carry out liquefaction susceptibility analyses which are more closely aligned with other types of analyses such as structural response. In particular, we can employ code-prescribed spectral loads exactly as are used by structural designers. This leads to an analysis of liquefaction which is consistent with other earthquake engineering practice in New Zealand.

INTRODUCTION

The purpose of the work described below is to create a methodology for analysis of liquefaction susceptibility which is consistent with other earthquake engineering design practice currently in use in New Zealand. To this end, we propose an analysis which uses ground surface response spectra as the basic measure of seismic loading. These spectra may be taken directly from the New Zealand Loadings Code, and the resulting characterisation of liquefaction hazard will be completely consistent with other current forms of analysis and design. Use of the basic elastic ($\mu = 1$) acceleration response from the loadings code gives a determination of liquefaction hazard appropriate for ground shaking levels having a less than ten percent probability of exceedance in 50 years.

In order to make effective use of ground surface response spectra in liquefaction analysis, we will adopt two widely used modeling procedures. First we will assume seismic pore pressure generation is directly related to the dissipated energy density in the soil deposit in question. Second, we will calculate the dissipated energy density using quasi-linear site response techniques similar to those used in nearly all site response studies.

A relationship between pore pressure increase due to ground shaking and dissipated energy was first proposed by Nemat-Nasser and Shokooh [1] in 1979. Their ideas were extended by Davis and Berrill [2], Berrill and Davis [3], and Simcock, *et.al.* [4] during the period 1982-85. Further research was carried out by Law, *et.al.* [5] and reported by Wang and Law [6] in 1994. Most recently, Trifunac [7] and Figueroa *et.al.* [8,9] have employed dissipated energy analyses to assess liquefaction hazard.

The second link in our modeling process is to calculate the amount of dissipated energy per unit volume of soil in the soil layer in question, based upon a prescribed acceleration response spectrum at the ground surface. Several steps are required to accomplish this objective. First we will use the given acceleration response spectrum to estimate the ground surface Fourier displacement spectrum $U_o(\omega)$. We will then model the site soils as linear elastic materials with hysteretic damping in a similar fashion to widely used methods for site response analysis. Estimates for shear modulii and damping coefficients for all soils at the site may be obtained from compilations of data available in the literature. Finally we use Parseval's theorem to obtain the dissipated energy density in the soil deposit under scrutiny. All calculations are performed in the frequency domain. The method will be illustrated by worked examples..

One final point of considerable interest is raised in this paper. By approaching liquefaction from the conventional site response standpoint, we are in a position to account for the effects of soil layering, particularly those effects associated with resonance. In nearly all site response analyses, one is concerned with resonances which appear at the ground surface. However, resonance may occur at any depth within a stratified soil profile, and if it should happen to coincide with a

[1] *University of Canterbury, Christchurch*
[2] *Fellow*

liquefiable deposit, the effect may be to enhance the liquefaction potential of the site dramatically. Most existing liquefaction potential models consider the suspect soil in isolation. That is, no account is taken of the position of the deposit within the soil column, nor of the dynamic properties of the column as a whole. As a result, effects of resonance cannot be considered. The work presented here offers a unique way to incorporate the overall site dynamics into the assessment of liquefaction susceptibility.

PORE PRESSURE AND DISSIPATED ENERGY

The earliest liquefaction potential models were developed around the idea that the pore pressure generated by shaking was related to the cyclic shear stress supported by the soil. A summary of these developments may be found in Seed [10]. The pore pressure - shear stress relationship grew naturally from laboratory test data where stresses could be carefully controlled. An unfortunate aspect of these models was the fact that the stresses in the field during an earthquake were far from controlled, and certain empirical assumptions were necessary in order to obtain even rough estimates of cyclic stress levels. Nevertheless, these models found wide currency in practice, despite certain observational inconsistencies [11].

The suggestion that pore pressure may be directly related to the amount of seismic energy dissipated in the soil was put forward by Nemat-Nasser and Shokooh [1]. Their reasoning stemmed from the idea that shaking a loose dry granular soil results in densification which must be accompanied by energy dissipation. Then if the soil were saturated rather than dry, the pore pressure to resist densification may itself be a manifestation of the energy dissipation. Their idea was used by Davis and Berrill [2] who proposed a simple linear relationship between pore pressure and dissipated energy, and combined that with a simplified earthquake energy attenuation model, to produce a complete theory of liquefaction evaluation based on earthquake magnitude, epicentral distance, and site soil characteristics. Subsequently, cyclic triaxial tests with precise measurements of dissipated energy were carried out by Simcock *et.al.* [4] to investigate what form of relationship might exist. These tests led to a revised liquefaction model by Berrill and Davis [3]. Subsequently Law *et.al.* [5] carried out a sequence of cyclic loading tests similar to those of Simcock's, and proposed a liquefaction model similar to that in [3]. In [7], Trifunac refined the original models proposed in [2] and [3] by incorporating more sophisticated energy attenuation relationships to eliminate certain anomalous results associated with short epicentral distances. No new data concerning the pore pressure - dissipated energy relationship is contained in [7]. The work of Figueroa *et.al.* [8,9], while presenting data on the total dissipated energy required to produce liquefaction, also gives no detailed information on the pore pressure - energy relationship.

Letting p denote pore pressure due to shaking and D dissipated energy density, the simplest relationship we can envision is linear

$$p = \alpha D \tag{1a}$$

where α is a dimensionless constant. A more elaborate nonlinear model is [3,5]

$$\frac{p}{\sigma'_o} = \alpha \left(\frac{D}{\sigma'_o} \right)^{\beta} \tag{1b}$$

where α and β are constants. Comparisons of both forms of equation (1) with experimental data may be found in references 3 and 5. While equation (1a) is clearly a rough approximation to experimental data, it has the advantage of simplicity, and its lack of precision is felt to be more in keeping with the uncertainty associated with other aspects of the modeling procedure. Thus we propose to use the linear form of equation (1a) to characterise pore pressure increase due to seismic ground motions.

ESTIMATION OF FOURIER DISPLACEMENT SPECTRA

As a first step toward calculation of the dissipated energy D, we wish to characterise the site motions via the Fourier displacement amplitude spectrum denoted $U_o(\omega)$. Here we use ω to represent frequency. To begin we assume the undamped ground surface acceleration response spectrum, denoted $S_a(\omega)$, is known. Then the corresponding pseudo-velocity spectrum is given by

$$PS_v(\omega) = \frac{1}{\omega} S_a(\omega)$$

It is well known that PS_v is an upper bound for the Fourier amplitude of acceleration. Thus

$$\left\| \omega^2 U_o(\omega) \right\| \le PS_v(\omega)$$

where $U_o(\omega)$ denotes the ground surface displacement spectrum, and we have used the fact that the Fourier acceleration is ω^2 times the Fourier transform of displacement. Combining the previous two equations, we find

$$\left\| U_o(\omega) \right\| \le S_a(\omega) / \omega^3 \tag{2}$$

We will employ equation (2) with an = sign instead of $\le$ in the analysis below. The result is a conservative estimate for the input motion.

In the New Zealand Loadings Code NZS4203:1992, the basic elastic response spectrum is closely approximated by

$$S_a(T) = \begin{cases} 0.61\,g & for \quad T \le 0.6\,\text{sec} \\ 0.45\,g / T^{0.6} & for \quad 0.6\,\text{sec} \le T \le 1.0\,\text{sec} \\ 0.45\,g / T & for \quad 1.0\,\text{sec} \le T \end{cases} \tag{3}$$

where T represents period. Using equation (3) in equation (2) with $T = 2\pi / \omega$, we find

$$\left\| U_o(\omega) \right\| = \begin{cases} 0.72 / \omega^2 & for \quad \omega \le 6.28\,\text{sec}^{-1} \\ 1.50 / \omega^{2.4} & for \quad 6.28 \le \omega \le 10.47\,\text{sec}^{-1} \\ 6.10 / \omega^3 & for \quad 10.47\,\text{sec}^{-1} \le \omega \end{cases} \tag{4}$$

Equation (4) is the Fourier displacement spectrum which is consistent with the New Zealand Loadings Code. In light of our aim in this paper, it is appropriate to make certain modifications to (4). First, note that the acceleration spectrum given by equation (3) corresponds to 5 percent structural damping. While this is appropriate for structure loads, our objective is different: The undamped spectrum is desired for calculation of dissipated energy. In an average sense, the effect of 5 percent damping on typical acceleration response at a period of roughly 1 second is to halve the undamped acceleration. Thus we will double the coefficients in (4) to approximate the undamped Fourier displacement spectrum. Next, we note that for purposes of calculation of dissipated energy, two horizontal components of motion will be present. The spectrum given by (3) represents the strongest motion, but there will inevitably be motions in the orthogonal direction. Many materials codes, including some in New Zealand, specify the orthogonal motion as being 30 percent as strong as the strongest motion. As a result we will correct for bi-directionality by further multiplying the coefficients in (4) by a factor of 1.3. Next, note that for low frequencies, the spectrum $U_o(\omega)$ specified in (4) can grow without bound. In fact, displacements will be bounded and we will set a limiting Fourier displacement for low frequencies equal to $2\ m \times \sec$ corresponding to the value obtained from Brune's attenuation model [12,13] for a 7.5 magnitude earthquake with hypocentral distance of 12 *km*. With these corrections, equation (4) now becomes

$$\|U_o(\omega)\| = \begin{cases} 2.00 & \text{for } \omega \le 0.967 \text{ sec}^{-1} \\ 1.87/\omega^2 & \text{for } 0.967 \le \omega \le 6.28 \text{ sec}^{-1} \\ 3.90/\omega^{2.4} & \text{for } 6.28 \le \omega \le 10.47 \text{ sec}^{-1} \\ 15.86/\omega^3 & \text{for } 10.47 \text{sec}^{-1} \le \omega \end{cases} \quad (5)$$

The ground surface Fourier spectrum specified by (5) will be used in the example problems considered below. A graph of equation (5) is shown in Figure 1. In the integrations given below, we have truncated the spectrum for both low and high frequencies. Our low frequency cut-off is 0.10 sec^{-1}. The response at lower frequencies than this has insignificant effect on the dissipated energy calculations. For our high frequency cut-off, we take 100 sec^{-1}. At frequencies higher than this, the hysteretic damping model we employ below becomes increasingly inappropriate. Finally, note the coefficients in equation (5) are sensitive to dimensions. We have ω in 1/sec and U_o in $m \times \sec$.

CALCULATION OF DISSIPATED ENERGY

We will begin by considering a homogeneous soil profile as this will serve to illuminate the mathematics. Subsequently we will generalise our results to multilayered situations. In all cases we consider only vertically propagating, horizontally polarized shear waves.

Consider the homogeneous halfspace composed of viscoelastic soil with hysteretic damping shown in Figure 2. Let x denote depth measured from the free surface and let $u = u(x,t)$ be horizontal displacement. Then the shear strain is

$$\gamma(x,t) = \partial u(x,t)/\partial x \quad (6)$$

The corresponding shear stress is given by

$$\tau(x,t) = G\gamma(x,t) + d\frac{\partial \gamma(x,t)}{\partial t} \quad (7)$$

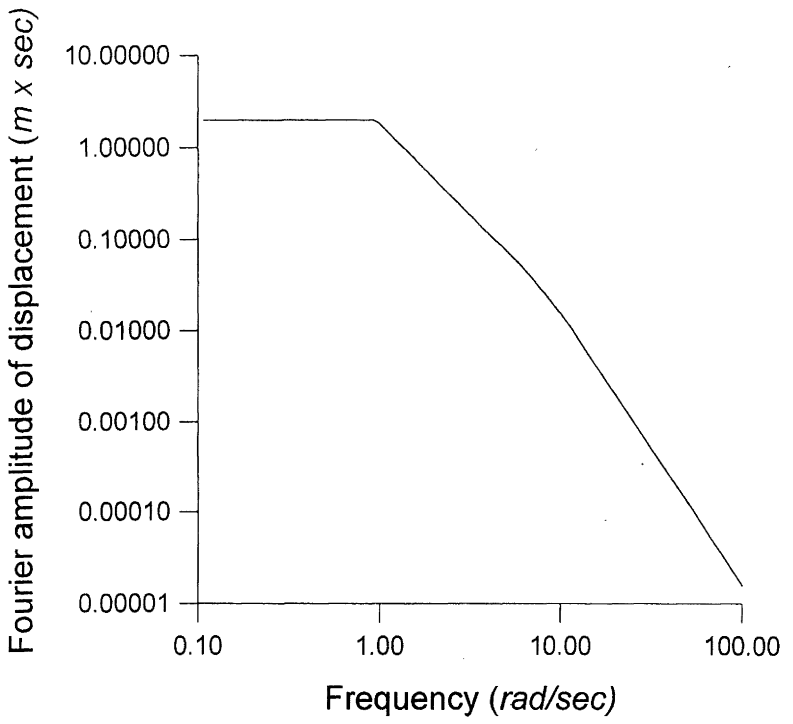

FIGURE 1 Ground surface displacement spectrum

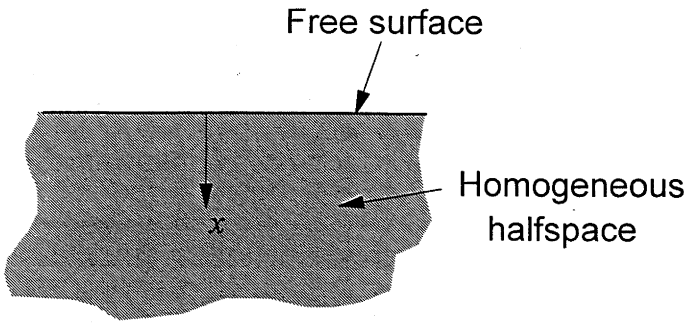

FIGURE 2 Homogeneous deposit of visco-elastic soil

where G denotes shear modulus and d is a damping coefficient. We make the common assumption of viscous frequency independent damping so that

$$d = \frac{2G\eta}{|\omega|} \tag{8}$$

where η is the constant damping ratio. Finally we introduce the equilibrium equation

$$\frac{\partial \tau(x,t)}{\partial x} = \rho \frac{\partial^2 u(x,t)}{\partial t^2} \tag{9}$$

Combining (6) - (9) we have

$$G\left[\frac{\partial^2 u(x,t)}{\partial x^2} + \frac{2\eta}{|\omega|}\frac{\partial^3 u(x,t)}{\partial x^2 \partial t}\right] = \rho \frac{\partial^2 u(x,t)}{\partial t^2} \tag{10}$$

Equation (6) - (10) set out the mathematics for vertically propagating *SH* waves. They are common to nearly all ground response analyses.

It is convenient now to move into the frequency domain. Let $U(x,\omega)$ be the Fourier transform of $u(x,t)$. We will use the notation $u(x,t) \leftrightarrow U(x,\omega)$ to identify a Fourier pair. We transform equation (10) to obtain

$$c^2(1+2i\eta)\frac{\partial^2 U(x,\omega)}{\partial x^2} + \omega^2 U(x,\omega) = 0 \tag{11}$$

where $c^2 = G/\rho$ is the shear wave velocity squared. Equation (11) has this solution

$$U(x,\omega) = A(\omega)e^{ikx} + B(\omega)e^{-ikx} \tag{12}$$

where k is the complex wave number

$$k = \frac{\omega/c}{\sqrt{1+2i\eta}} \tag{13}$$

The stress free boundary condition at $x = 0$ results in $\partial U(x,\omega)/\partial x = 0$. Applying this condition to equation (12) gives $A(\omega) = B(\omega)$. Hence (12) can be written

$$U(x,\omega) = U_o(\omega)\cos kx \tag{14}$$

where $U_o(\omega) = 2A(\omega)$ is the Fourier transform of the free surface displacement time history. That is $u_o(t) \leftrightarrow U_o(\omega)$. We will assume $U_o(\omega)$ is given by equation (5) although any other surface motion could be used as well.

Next, for any given ground motion, the dissipated energy density $D(x)$ at any given depth x is found by integrating in the time domain

$$D(x) = \int_{-\infty}^{\infty} \mathrm{Re}(\tau_d(x,t))\,\mathrm{Re}\left(\frac{\partial \gamma(x,t)}{\partial t}\right)dt \tag{15}$$

where τ_d is the anelastic stress

$$\tau_d = \frac{2G\eta}{|\omega|}\frac{\partial^2 u(x,t)}{\partial x \partial t}. \tag{16}$$

In (15), the limits of integration need only extend over the duration of shaking, but these have been expanded to cover the entirety of time assuming the motion is zero everywhere outside the earthquake duration. Together equations (15) and (16) give

$$D(x) = \int_{-\infty}^{\infty} \frac{2G\eta}{|\omega|}\left[\mathrm{Re}\left(\frac{\partial^2 u(x,t)}{\partial x \partial t}\right)\right]^2 dt \tag{17}$$

Next we want to make use of Parseval's theorem [14]. For any complex functions $f(t)$ and $g(t)$, we have the following

$$\int_{-\infty}^{\infty}\mathrm{Re}(f(t))\,\mathrm{Re}(g(t))dt = \frac{1}{2\pi}\int_{-\infty}^{\infty}\frac{1}{2}(G(\omega) + G^*(-\omega)) \times \frac{1}{2}(F(-\omega) + F^*(\omega))d\omega \tag{18}$$

Here $f(t) \leftrightarrow F(\omega)$ and $g(t) \leftrightarrow G(\omega)$. The $*$ implies complex conjugate.

Now returning attention to equation (17), we note that

$$\frac{\partial^2 u(x,t)}{\partial x \partial t} \leftrightarrow i\omega \frac{\partial U(x,\omega)}{\partial x}.$$

Also, from equation (14) we have

$$\frac{\partial U(x,\omega)}{\partial x} = -U_o(\omega)k\sin kx$$

$$\frac{\partial U(x,-\omega)}{\partial x} = -U_o^*(\omega)k\sin kx$$

$$\left(\frac{\partial U(x,\omega)}{\partial x}\right)^* = -U_o^*(\omega)(k\sin kx)^*$$

$$\left(\frac{\partial U(x,-\omega)}{\partial x}\right)^* = -U_o(\omega)(k\sin kx)^*$$

where we have used $U_o(-\omega) = U_o^*(\omega)$ due to $u_o(t)$ being real valued. With the help of the above relationships, we can apply the form of Parseval's theorem in (18) to equation (17) in order to have

$$D(x) = \frac{1}{2\pi}\int_{-\infty}^{\infty} \frac{2G\eta\omega^2}{|\omega|}\|U_o(\omega)\|^2[\mathrm{Re}(k\sin kx)]^2\,d\omega \qquad (19)$$

Equation (19) allows us to calculate the dissipated energy density at any depth x within a homogenous soil profile. Note that the computations occur strictly in the frequency domain.

We can now turn attention to the more likely situation where a multilayered soil profile exits at our site. Figure 3 illustrates this condition. We assume horizontal layering with homogeneous soil properties within each individual layer. The layers are of thickness h_m, numbered sequentially downward from the ground surface. We begin by considering the response of one layer, say layer m, as illustrated in Figure 4. Let x be a local coordinate measured vertically downward from the upper surface of the layer. In this coordinate system the equations of motion are exactly the same as equations (6) through (10) for the homogeneous soil profile. The only difference is one of boundary conditions.

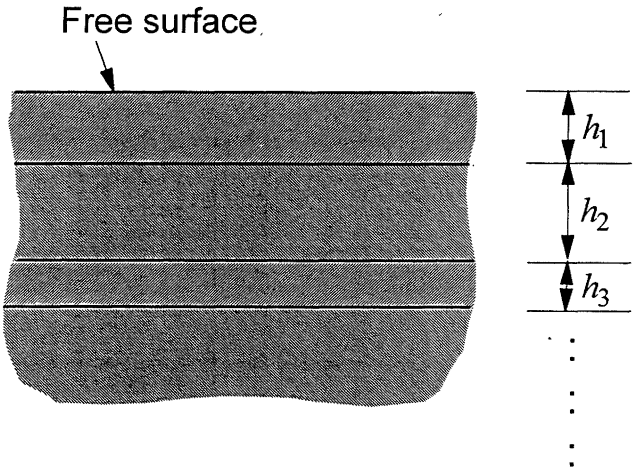

FIGURE 3 Layered soil profile

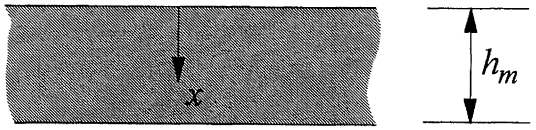

FIGURE 4 Details of layer m

Moving into the frequency domain, the Fourier displacement for the layer will obey an equation similar to (11), and the solution will be

$$U(x,\omega) = A(\omega)\exp(ik_m x) + B(\omega)\exp(-ik_m x) \qquad (20)$$

where

$$k_m = \frac{\omega/c_m}{\sqrt{1+2i\eta_m}} \qquad (21)$$

is the complex wave number for layer m. Here η_m and c_m are the damping and shear wave velocity for the layer. Equations (20) and (21) are the m-layer counterparts to (12) and (13).

Next let $T(x,\omega) \leftrightarrow \tau(x,t)$ be the Fourier transform of the shear stress. Then transforming equation (7) and using equation (20) in the result gives

$$T(x,\omega) = iG_m k_m(1+2i\eta_m)[A(\omega)\exp(ik_m x) - B(\omega)\exp(-ik_m x)] \qquad (22)$$

Now we can relate the displacement and stress at the upper surface of the layer to the displacement and stress at the layer base using a transfer matrix. Let $U_1 = U(0,\omega)$ be the upper surface displacement and $T_1 = T(0,\omega)$ be the corresponding stress. Similarly let U_2 and T_2 be evaluated at $x = h_m$, the layer base. Then after some manipulation

$$\begin{bmatrix} U_2 \\ T_2 \end{bmatrix} = \begin{bmatrix} J_{11} & J_{12} \\ J_{21} & J_{22} \end{bmatrix} \times \begin{bmatrix} U_1 \\ T_1 \end{bmatrix} \qquad (23)$$

where the transfer matrix **J** has components

$$\begin{aligned} J_{11} &= \cos k_m h_m = J_{22} \\ J_{12} &= \frac{1}{R_m}\sin k_m h_m \\ J_{21} &= -R_m \sin k_m h_m \end{aligned} \qquad (24)$$

and

$$R_m = G_m k_m(1+2i\eta_m) \qquad (25)$$

It is now a simple matter to find the response at any point in the soil profile. We construct transfer matrices $\mathbf{J_m}$ for each layer . Multiplying these we can build up a composite matrix taking us from anywhere in the profile (say layer n) to the free surface. The result is

$$\begin{bmatrix} U_n \\ T_n \end{bmatrix} = \begin{bmatrix} H_{11} & H_{12} \\ H_{21} & H_{22} \end{bmatrix} \times \begin{bmatrix} U_o \\ 0 \end{bmatrix} \qquad (26)$$

where the matrix **H** is given by the product of the **J** matrices:

$$\mathbf{H} = \mathbf{J_n} \times \mathbf{J_{n-1}} \times \cdots \times \mathbf{J_1} \qquad (27)$$

On the left side of equation (26) are the Fourier displacement and stress at the base of layer n. On the right hand side are the **H** matrix and the vector of the Fourier displacement and the *zero* stress at the ground surface. In equation (26), U_o is the known surface displacement $U_o(\omega)$ given in equation (5).

Once U_n and T_n are determined, we can calculate the dissipated energy density for layer n. The calculations are parallel to those linking equations (17) and (19) in the homogeneous soil case. Omitting details, the final result is

$$D_n = \frac{1}{2\pi}\int_{-\infty}^{\infty} \frac{2G_n\eta_n\omega^2}{|\omega|}\|U_o(\omega)\|^2\left[\mathrm{Re}\left(\frac{H_{21}(\omega)}{G_n(1+2i\eta_n)}\right)\right]^2 d\omega \qquad (28)$$

Note that only one component of the **H** matrix is needed for this calculation. For the special case where $n=1$, we have

$$H_{21} = J_{21} = -R_1 \sin k_1 h_1 = -G_1 k_1(1+2i\eta_1)\sin k_1 h_1$$

and use of this result in (28) leads back to our expression for the homogeneous soil case, equation (19). Note also that (28) gives the dissipated energy density at the base of layer n. In general, the dissipated energy at any depth in the layer may be found by using the appropriate dimension. Despite the fact (28) appears to be complicated, the calculations are relatively simple and straightforward. The shear modulii, damping coefficients, and layer thicknesses are first used to construct the layer **J** matrices. Then the **J**'s are multiplied to find **H**. Finally the integration is carried out to give the dissipated energy. Equation (28) is the main result of this paper. When used with equation (1), it provides a rational approximation for the pore pressure increase in any layer of a stratified soil profile.

EXAMPLE CALCULATION

In this section we will work through a typical calculation and discuss the various parameter values required. A hypothetical soil profile is given in Table 1. For simplicity, we assume all five soil layers have the same density, $2.0\ t/m^3$, and we assume the water table is located at the ground surface. In Table 1, the column marked G_{max} gives assumed values for the average small strain, elastic shear modulus for each layer. The values shown are typical of the range of shear modulii found in soils at shallow depths.

The calculation of dissipated energy density and pore pressure increase takes place in two steps. The first step is to obtain values of non-linear dynamic shear modulii and damping coefficients for all layers due to the specified ground surface motion. This can be accomplished by use of any of the many ground response analyses such as SHAKE [15] and leads to the values of G and η shown in the fifth and sixth columns of Table 1. The particular values shown were obtained using a simplified Haskell-Thomson transfer matrix analysis [16] combined with the analytical shear modulus and damping ratio representations of Ishibashi and Zhang [17]. The ground surface motions were specified by equation (5). It should be noted that so-called 'top-down' analyses, in which the control motion is specified at the ground surface, will not always converge. This is in contrast to 'bottom- up' analyses, where the control motion is specified at basement rock, and which must converge regardless of how strong the input motions are. It is a somewhat unfortunate aspect of the method proposed here that a top-down analysis is required. A discussion of convergence of top-down calculations may be found in Kausel and Roesset [18].

The second step in our calculation is to use equation (28) to find the dissipated energy density and then equation (1a) to determine the increase in pore pressure at any specified depth. These computations are performed using the shear modulii and damping values obtained in step 1, together with the surface displacement spectrum specified in equation (5). For the purposes of our example, we have taken the dimensionless constant α in equation (1a) to be 80. This value is based on the test data of Simcock *et.al.*[4]. A somewhat smaller value for α might be appropriate if the data of Law *et.al.* [5] are also considered. It seems evident additional test data are needed to clarify the best value for α.

Results for our example soil profile are illustrated in Figure 5. Computations of dissipated energy density and pore pressure increase were made at depth intervals of 0.1 m throughout the soil profile. Figure 5 shows the pore pressure increase as well as the initial effective stress profile which has a constant slope due to the uniform density of all layers and the location of the water table at the ground surface. It is clear liquefaction has been predicted in layer 3, the pore pressure increase being equal or greater than the initial effective stress throughout the layer. None of the other layers exhibit a tendency toward liquefaction. Note that the pore pressure increase first equals the initial effective stress at the top of the layer, predicting that liquefaction initiates at the layer top and then propagates downwards as has been observed in laboratory experiments [19,20].

The results illustrated in Figure 5 depend strongly on both computational steps noted above. The ground response analysis leads to the dynamic shear modulus and damping ratio values which in turn play an important role in determining the dissipated energy density. Small changes in the initial data for the site may result in important differences in both computational steps. It is interesting therefore to alter the parameters of our example problem slightly to illustrate the importance of the details of site stratigraphy. Table 2 shows the relevant data for our altered problem. In terms of initial data, only the thickness of layer 2 has been altered: from 2.5 m thick to 5.0 m thick.

With the exception of layer 1, the ground response analysis now gives significantly different results for the dynamic shear modulii and damping coefficients. Layer 3 still suffers the greatest amount of softening, but not so much as occurred previously. If we now use these data to calculate the dissipated energy density and pore pressure increase, the pore pressure profile shown in Figure 6 results. Note that the induced pore pressure in layer 3 is much smaller than previously, being roughly one-half the increase seen in Figure 5. Clearly liquefaction is not predicted here. The difference between Figures 5 and 6 results solely from the change in thickness of layer 2.

Most existing liquefaction susceptibility models base their predictions on only two sets of data: one set concerning the

Table 1. Example Soil Profile

Layer number	Thickness (m)	$\rho\ (t/m^3)$	$G_{max}\ (kPa)$	$G(kPa)$	η
1	5.0	2.0	50,000	37,258	0.057
2	2.5	2.0	100,000	47,785	0.131
3	2.5	2.0	50,000	4,357	0.290
4	2.5	2.0	100,000	13,945	0.265
5	7.5	2.0	250,000	45,183	0.246

Table 2. Altered data for example problem

Layer number	Thickness (m)	ρ (t/m^3)	G_{max} (kPa)	$G(kPa)$	η
1	5.0	2.0	50,000	37,258	0.057
2	5.0	2.0	100,000	50,706	0.122
3	2.5	2.0	50,000	13,207	0.211
4	2.5	2.0	100,000	39,516	0.160
5	7.5	2.0	250,000	138,756	0.107

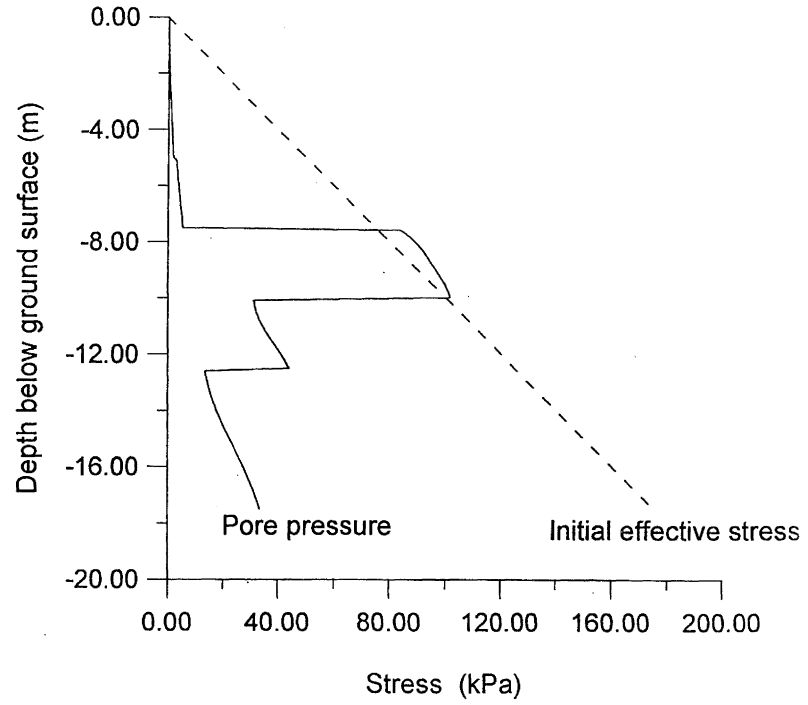

FIGURE 5 Excess pore pressure profile

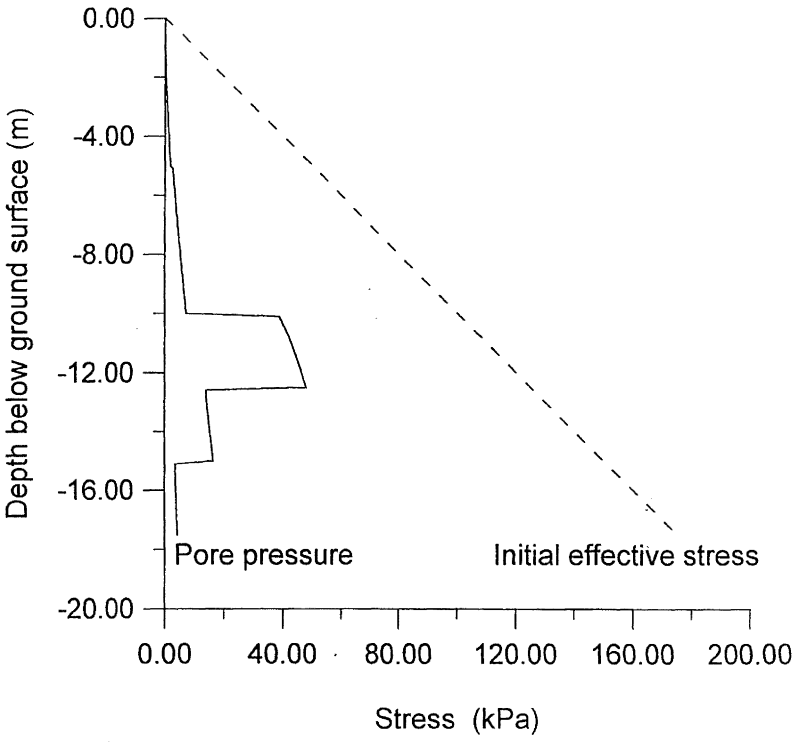

FIGURE 6 Pore pressure profile for deeper layer

soil in question (SPT value, grain size, initial effective stress, etc.), and the second set concerning the earthquake (magnitude, epicentral distance, etc.). These models generally do not consider the possibility of neighboring soil layers affecting the response and liquefaction potential of the particular soil in question. The calculations we have performed above indicate clearly that neighboring soils should be considered. One can intuitively examine this effect by considering a situation in which a loose layer of sand is found between two very stiff soil layers. As shear waves propagate upward through the soils, the stiff layers will tend to reflect seismic wave energy back into the soft layer. The soft layer acts somewhat like a wave guide and energy will accumulate there as a resonance effect. The amount of dissipated energy will be large and liquefaction likely. In contrast, the same loose sand between two softer layers will not experience this trapping of energy, and liquefaction may not occur.

As a final comment, we note that drainage from adjacent layers may also have a significant effect on the increased pore pressure, and hence the likelihood of liquefaction, in a particular sand layer. This aspect of the problem cannot be directly considered by our analysis. The analysis used here is confined to the frequency domain while the problem of drainage between layers must be considered in the time domain.

CONCLUSION

In this paper we have attempted to construct a liquefaction susceptibility model which is consistent with other design practice in New Zealand. Using a transfer matrix approach, the calculation of dissipated energy density in a multilayered soil profile due to specified surface motion has been considered in detail. Pore pressure increase at any depth within the profile is determined from the dissipated energy. A predicted profile of excess pore pressure may be constructed for all the site soils. The likelihood of liquefaction in any soil layer is clearly indicated by the method. If the specified surface motion is taken from the loadings code, the entire analysis is consistent with the code and hence with other elements of structural design.

Unlike existing liquefaction models, our method incorporates the effects of all soil layers and can indicate when resonance effects may lead to exaggerated deformations and enhanced liquefaction potential. The effects of site stratigraphy may significantly affect the likelihood of liquefaction of any individual soil layer, and should be considered in any liquefaction susceptibility analysis.

REFERENCES

1. Nemat-Nasser, S. and Shokooh, A., 1979 'A unified approach to densification and liquefaction of cohesionless sand in cyclic shearing', *Canadian Geotech. Jour.*, 16:59-678.

2. Davis, R.O. and Berrill, J.B. 1982. 'Energy dissipation and seismic liquefaction in sands', *Earthq. Engg. Struct. Dyns.*, 10:59-68.

3. Berrill, J.B. and Davis, R.O. 1985. 'Energy dissipation and seismic liquefaction in sands: Revised model', *Soils and Founds.*, 25(2):106-118.

4. Simcock, K.J., Davis, R.O., Berrill, J.B. and Mullenger, G. 1983. 'Cyclic triaxial tests with continuous measurement of dissipated energy', *Geotech. Testing Jour.*, 6:35-39.

5. Law, K.T., Cao, Y.L. and He, G.N. 1990. 'An energy approach for assessing seismic liquefaction potential', *Canadian Geotech. Jour.*, 27:320-329.

6. Wang, J.G.Z.Q. and Law, K.T. 1994. *Siting in Earthquake Zones*, Balkema, Rotterdam, 115pp.

7. Trifunac, M. 1995. 'Empirical criteria for liquefaction in sands via standard penetration tests and seismic wave energy', *Soil Dyns. Earthq. Engg.*, 14:419-426.

8. Figueroa, J.L., Saada, A.S., Liang, L. and Dahisaria, M.N. 1994. 'Evaluation of soil liquefaction by energy principles', *Jour. Geotech. Engg. Div.*, ASCE, 120:1554-1569.

9. Liang, L., Figueroa, J.L. and Saada, A.S. 1995. 'Liquefaction under random loading: Unit energy approach', *Jour. Geotech. Eng. Div.*, ASCE, 121:776-781.

10. Seed, H.B. 1979. 'Soil liquefaction and cyclic mobility evaluation for level ground during earthquakes', *Jour. Geotech. Engg. Div.*, ASCE, 105:210-255.

11. Davis, R.O. and Berrill, J.B. 1983. 'Comparison of a liquefaction theory with field observations', *Geotechnique*, 33:455-460.

12. Brune, J.N. 1970. 'Tectonic stress and the spectra of seismic shear waves from earthquakes', *Jour. Geophys. Res.*, 75:4997-5009.

13. Brune, J.N. 1971. 'Correction', *Jour. Geophys. Res.*, 76:5002.

14. Bendat, J.S. and Piersol, A.G. 1980. *Engineering Applications of Correlation and Spectral Analysis*, John Wiley, New York.

15. Schnabel, P.B.,Lysmer, J. and Seed, H.B. 1972. 'SHAKE - a computer program for earthquake response analysis of horizontally layered sites', *Report No. EERC 72-12*, Earthquake Engineering Research Center, University of California, Berkeley.

16. Haskell, N.A. 1960. 'Crustal reflection of plane *SH* waves', *Jour. Geophys. Res.*, 65:4147-4150.

17. Ishibashi, I. and Zhang, X. 1993. 'Unified dynamic shear moduli and damping ratios of sand and clay', *Soils and Foundations*, 33(1):182-191.

18. Kausel, E. and Roesset, J.M. 1984. 'Soil amplification: Some refinements', *Soil Dyns. Earthq. Engg.*, 3:116-123.

19. Florin, V.A. and Ivanov, P.L. 1961. 'Liquefaction of saturated sandy soil', *Proc. 5th Int. Conf. Soil Mech. Found. Engg.*, Paris, 1:107-111.

20. Scott, R.F. and Zuckerman, K.A. 973. 'Sand blows and liquefaction', *The Great Alaskan Earthquake of 1964 - Engineering Volume*, Committee on the Alaska Earthquake, Division of Earth Sciences, National Research Council, National Academy of Sciences, Washington, D.C., 179-189.